Inorg. Chem. **2009**, *48*, 1309−1322

Induction of Cell Death by Ternary Copper(II) Complexes of L-Tyrosine and Diimines: Role of Coligands on DNA Binding and Cleavage and Anticancer Activity

Sethu Ramakrishnan,[†] Venugopal Rajendiran,[†] Mallayan Palaniandavar,*[,†] Vaiyapuri Subbarayan Periasamy,[‡] Bangalore Suresh Srinag,[§] Hanumanthappa Krishnamurthy,[§] and Mohammad Abdulkader Akbarsha[‡]

School of Chemistry and Department of Animal Science, School of Life Sciences, Bharathidasan University, Tiruchirapalli 620 024, India, and National Centre for Biological Science, Tata Institute for Fundamental Research, Bangalore 560 065, India

Received June 20, 2008

The mononuclear mixed ligand copper(II) complexes of the type [Cu(L-tyr)(diimine)](ClO_4), where tyr is L-tyrosine and diimine is 2,2′-bipyridine (bpy) (**1**), 1,10-phenanthroline (phen) (**2**), 5,6-dimethyl-1,10-phenanthroline (5,6-dmp) (**3**), and dipyrido[3,2-*d*:2′,3′-*f*]quinoxaline (dpq) (**4**), have been isolated and characterized by analytical and spectral methods. In the X-ray crystal structure **3** Cu(II) possesses a distorted square pyramidal coordination geometry with the two nitrogen atoms of 5,6-dmp ligand and the amine nitrogen and carboxylate oxygen atoms of L-tyrosine located at the equatorial sites and the coordinated water molecule present in the apical position. The electronic absorption and electron paramagnetic resonance (EPR) spectral parameters reveal that the complexes retain their square-based geometries even in solution. All of the complexes display a ligand field band in the visible region (600−700 nm) in Tris−HCl/NaCl buffer (5:50 mM) at pH 7.2 and also axial EPR spectra in acetonitrile at 77 K with $g_{\|} > g_{\perp}$ indicating a $d_{x^2-y^2}$ ground state. The $g_{\|}$ and $A_{\|}$ values of 2.230 and (170−180) $\times$ 10^{-4} cm^{-1}, respectively, conform to a square-based CuN_3O coordination chromophore, which is consistent with the X-ray crystal structure of **3**. The interaction of the complexes with calf thymus DNA (CT DNA) has been explored by using physical methods to propose modes of DNA binding of the complexes. Absorption (K_b) and emission spectral studies and viscosity measurements indicate that **4** interacts with DNA more strongly than all of the other complexes through partial intercalation of the extended planar ring of dpq with DNA base stack. Interestingly, complex **3** exhibits a DNA binding affinity that is higher than that of **2**, which suggests the involvement of 5,6-dimethyl groups on the phen ring in hydrophobic interaction with DNA surface. In contrast with the increase in relative viscosities of DNA bound to **2**−**4**, the viscosity of DNA bound to **1** decreases, indicating the shortening of the DNA chain length by means of the formation of kinks or bends. All complexes exhibit effective DNA (pUC19 DNA) cleavage at 100 μM complex concentrations, and the order of DNA cleavage ability varies as **3** > **2** > **4** > **1**. Interestingly, **3** exhibits a DNA cleavage rate constant that is higher than that of the other complexes only at 100 μM concentration, whereas **4** exhibits the highest cleavage rate constant at 80 μM complex concentration. The oxidative DNA cleavage follows the order **4** > **3** > **2** > **1**. Mechanistic studies reveal that the DNA cleavage pathway involves hydroxyl radicals. Interestingly, only **4** displays efficient photonuclease activity upon irradiation with 365 nm light, which occurs through double-strand DNA breaks involving hydroxyl radicals. Furthermore, cytotoxicity studies on the nonsmall lung cancer (H-460) cell line show that the IC_{50} values of **2**−**4** are more or less equal to cisplatin for the same cell line, indicating that they have the potential to act as very effective anticancer drugs in a time-dependent manner. The study of cytological changes reveals the higher induction of apoptosis and mitotic catastrophe for **4** and **3**, respectively. The alkaline single-cell gel electrophoresis (comet assay), DNA laddering, and AO/EB and Hoechst 33258 staining assays have also been employed in finding the extent of DNA damage. Flow cytometry analysis shows an increase in the percentage of cells with apoptotic morphological features in the sub-G_0/G_1 phase for **4**, whereas it shows mitotic catastrophe for **3**.

Introduction

Cisplatin is a widely used and well-known metal-based drug for cancer therapy, but it possesses inherent limitations such as side effects and low administration dosage. Therefore, attempts are being made to replace this drug with suitable alternatives, and numerous transition-metal complexes are synthesized and screened for their anticancer activities. Next to Ru(II) complexes, Cu(II) complexes are regarded as the most promising alternatives to cisplatin as anticancer substances. Copper(II) is known to play a significant role in biological systems and also as pharmacological agents.

* To whom correspondence should be addressed. E-mail: palanim51@yahoo.com.
[†] School of Chemistry, Bharathidasan University.
[‡] Department of Animal Science, School of Life Sciences, Bharathidasan University.
[§] Tata Institute for Fundamental Research.

10.1021/ic801144x CCC: $40.75
Published on Web 01/13/2009

Synthetic copper(II) complexes have been reported to act as potential anticancer and cancer inhibiting agents,[1−3] and a number of copper complexes[4,5] have been found to be active both in vitro and in vivo. Very recently, Reedijk and coworkers have found that the complex [Cu^{II}(pyrimol)Cl] brings about efficient self-activated DNA cleavage and cytotoxic effects toward L1210 murine leukemia and A2780 human ovarian carcinoma cell lines.[6] Sadler and coworkers have observed[7] that mixed ligand bis(salicylato)copper(II) complexes with diimines as coligands exhibit cytotoxic and antiviral activities. Very recently, Ng and coworkers have prepared ternary copper(II) complexes of ethylenediaminediacetic acid (H_2edda) and 1,10-phenanthroline (phen), which strongly bind to DNA and also regulate apoptosis.[8] We have recently reported mixed ligand copper(II) complexes of diimines, which bind and cleave DNA and also exhibit anticancer activity that is more efficient than that of cisplatin.[9] The use of phen as the coligand in the above ternary complexes is of considerable interest because some of the phen-containing copper complexes exhibit biological as well as pharmacological properties.[10] We have also reported that mixed ligand Cu(II)[9] and Ru(II)[11,12] complexes exhibit prominent anticancer activities in which the diimine coligands play a pivotal role in the mechanisms underlying the induction of cell death. The mixed ligand palladium(II) and platinum(II) complexes containing amino acids have been shown to act as potential anticancer agents.[13,14]

The study of ternary copper(II) complexes of diimines and amino acids as anticancer drugs is of interest because copper is a bioessential element but only in traces, and also, amino acids are present in all biological systems. Also, these monopositive complexes are expected to be more lipophilic than the corresponding dicationic complexes, thereby providing for greater uptake by cells and hence an enhanced cytotoxicity. Very recently, Guo and coworkers have found

Scheme 1. Copper(II) Complexes **1**−**4** and the Diimine Coligands

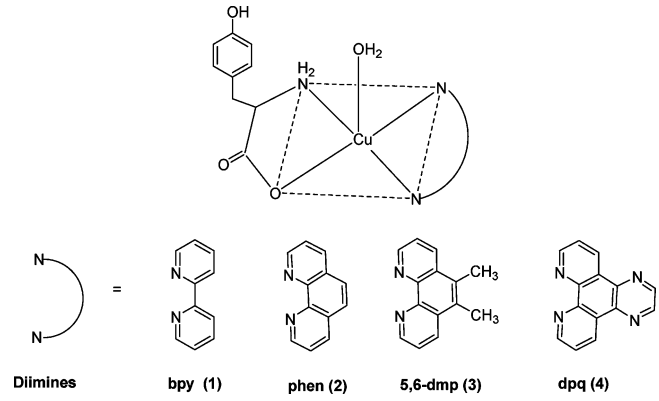

the ternary Cu(II) complex of phen and L-threonine to cleave DNA oxidatively and exhibit cytotoxicity.[15] In this Article, we have explored the cytotoxicity of mononuclear mixed ligand copper(II) complexes of the type [Cu(L-tyr)(diimine)](ClO_4) (**1**− **4**), where L-tyr is L-tyrosine and diimine is 2,2′-bipyridine (bpy) (**1**), 1,10-phenanthroline (phen) (**2**), 5,6-dimethyl-1,10-phenanthroline (5,6-dmp) (**3**), or dipyrido-[3,2-*d*:2′,3′-*f*]-quinoxaline (dpq) (**4**) (Scheme 1). It is generally believed that molecules, which damage DNA and block DNA synthesis indirectly through inhibition of biosynthesis of precursor molecules for nucleic acids or disrupt hormonal regulation of cell growth, would make them better candidates for development as anticancer agents.[16] Also, DNA has been identified as the possible primary molecular target[17] of metal-based anticancer agents such as cisplatin.[18] Therefore, we propose to investigate whether these complexes exhibit DNA binding and cleavage properties and thus can be candidates suitable for investigating in vitro cytotoxicity. The introduction of chirality via the amino acid may enhance the pharmacological behavior of the copper complexes by adopting a specific conformation and may also confer selective binding affinity for the chiral DNA. Furthermore, the carboxylate group of L-tyrosine has the potential to interact with sugar hydroxyl groups of DNA, to enhance the DNA binding affinity, and to provide recognition elements, thus leading to the selective control of the metal chelate−nucleobase recognition process. Also, there has been considerable attention focused on the use of the small metal complexes containing diimines as recognition elements of DNA[19−22] and metal-based synthetic nucleases.[22−24] The incorporation

(1) May, P. M.; Williams, D. R. Chapter 7. In *Metal Ions in Biological Systems*; Sigel, H., Ed.; Marcel Dekker: New York, 1981; Vol. *12*.
(2) *Metal Ions in Biological Systems*; Sigel, H., Ed.; Marcel Dekker: New York, 1981; Vol. *13*.
(3) Miura, T.; Hori-i, A.; Mototani, H.; Takeuchi, H. *Biochemistry* **1999**, *38*, 11560–11569.
(4) Fernandes, C.; Parrilha, G. L.; Lessa, J. A.; Santiago, L. J. M.; Kanashiro, M. M.; Boniolo, F. S.; Bortoluzzi, A. J.; Vugman, N. V.; Herbst, M. H.; Horn, A., Jr. *Inorg. Chim. Acta* **2006**, *359*, 3167–3176.
(5) Bales, B. C.; Kodama, T.; Weledji, Y. N.; Pitie, M.; Meunier, B.; Greenberg, M. M. *Nucleic Acid Res.* **2005**, *33*, 5371–5379.
(6) Uma Maheswari, P.; Roy, S.; Dulk, H. D.; Barends, S.; Wezel, G. V.; Kozlevcar, B.; Gamez, P.; Reedijk, J. *J. Am. Chem. Soc.* **2006**, *128*, 710–711.
(7) Ranford, J. D.; Sadler, P. J.; Tocher, D. A. *Dalton Trans.* **1993**, 3393–3399.
(8) Ng, C. H.; Kong, K. C.; Von, S. T.; Balraj, P.; Jensen, P.; Thirthagiri, E.; Hamada, H.; Chikira, M. *Dalton Trans* **2008**, 447–454.
(9) Rajendiran, V.; Karthik, R.; Palaniandavar, M.; Evans, H. S.; Periasamay, V. S.; Akbarsha, M. A.; Srinag, B. S.; Krishnamurthy, H. *Inorg. Chem.* **2007**, *46*, 8208–8221.
(10) Farrell, N. *Transition Metal Complexes as Drugs and Chemotherapeutic Agents*; Kluwer Academic: Dordrecht, The Netherlands, 1989; 2777−2795.
(11) Rajendiran, V.; Murali, M.; Suresh, E.; Sinha, S.; Somasundaram, K.; Palaniandavar, M. *Dalton Trans.* **2008**, 148–163.
(12) Rajendiran, V.; Murali, M.; Suresh, E.; Periasamay, V. S.; Akbarsha, M. A.; Palaniandavar, M. *Dalton Trans.* **2008**, 2157–2170.
(13) Jin, V. X.; Ranford, R. D. *Inorg. Chim. Acta* **2000**, *304*, 38.
(14) Wai-Yin sun, R.; Ma, D.; Ming, E. L.; Che, C. *Dalton Trans* **2007**, 4887–4892.
(15) Zhang, S.; Zhu, Y.; Tu, C.; Wei, H.; Yang, Z.; Lin, L.; Ding, J.; Zhang, J.; Guo, Z. *J. Inorg. Biochem.* **2004**, *98*, 2099–2106.
(16) *Cancer Chemotherapeutic Agents*; Foye, W. O., Ed.; American Chemical Society: Washington, DC, 1995.
(17) Vokes, E. E.; Weichselbaum, R. R.; Mick, R.; McEvilly, J. M.; Haraf, D. J.; Panje, W. R. *J. Natl. Cancer Inst.* **1992**, *84*, 877–882.
(18) Rose, P. G.; Bundy, B. N.; Watkins, E. B.; Thigpen, J. T.; Deppe, G.; Maiman, M. A.; Clarke-Pearson, D. L.; Insalaco, N. *Engl. J. Med.* **1999**, *340*, 1144–1153.
(19) Erkkila, K. E.; Odom, D. T.; Barton, J. K. *Chem. Rev.* **1999**, *99*, 447–454.
(20) Lincoln, P.; Nordén, B. *J. Phys. Chem. B* **1998**, *102*, 9583–9594.
(21) Onfelt, B.; Lincoln, P.; Nordén, B. *Proc. Natl. Acad. Sci. U.S.A.* **2000**, *97*, 5708–5713.
(22) Bales, B. C.; Pitie, M.; Meunier, B.; Greenberg, M. M. *J. Am. Chem. Soc.* **2002**, *124*, 9062–9063.
(23) Sigman, D. S.; Mazumder, A.; Perrin, D. M. *Chem. Rev.* **1993**, *93*, 2295–2316.

of methyl groups on the five and six positions of the phen ring would provide a hydrophobic recognition element,[25] and the fusion of an additional aromatic ring, as in dpq coligand, would show strong partial intercalation leading to enhancement of the DNA binding affinity,[26−30] the DNA cleavage efficiency, and possibly the cytotoxicity[9] of the complexes. Therefore, designing such suitable copper(II) complexes for DNA binding and cleaving under both oxidative and hydrolytic conditions is of remarkable importance in considering the advantages of processes that produce fragments similar to those formed by restriction enzymes.[31−33]

Lung cancer is a leading cause of cancer morbidity and mortality among men and women; over one million deaths due to malignant tumors of the lung and 1.2 million new cases of lung cancer occur worldwide each year, making it an epidemic disease,[34,35] and the currently used drug, cisplatin, is limited by its side-effects and cellular resistance. Therefore, we chose to screen the cytotoxic property of the DNA-cleaving copper(II) complexes toward H-460 human nonsmall lung cancer cell lines. It is remarkable that the complexes exhibit IC_{50} values that are more or less equal to cisplatin for the same cell line, which indicates that they are promising drugs for cancer. Furthermore, because drug-induced activation of specific signaling pathways concerned with controlled cell death or apoptosis has become a promising approach in cancer therapy,[16,36] the ability of the present complexes to regulate cell death has been investigated by adopting MTT assay, comet assay, DNA laddering, and cell cycle analysis. It is found that the 5,6-dmp and dpq complexes induce a higher percentage of cell death but through different modes of action.

Results and Discussion

Synthesis and Structures of Complexes. The mixed ligand copper(II) complexes of [Cu(L-tyr)(diimine)]ClO_4 (**1**−**4**), where L-tyr is L-tyrosine, and diimine is 2,2′-bipyridine (bpy) (**1**), 1,10-phenanthroline (phen) (**2**), 5,6-dimethyl-1,10-phenanthroline (5,6-dmp) (**3**), and dipyridoquinoxaline (dpq)[37] (**4**) have been isolated by the addition of a methanolic solution of hydrated copper(II) perchlorate to a mixture of deprotonated L-tyrosine and diimine in methanol. All complexes have been obtained in good yield. The X-ray crystal structures of **1**, **2**, and **4** have already been reported, and that of **3** has been determined in this study. All complexes are soluble in Tris−HCl/NaCl (5:50 mM) buffer at pH 7.1.

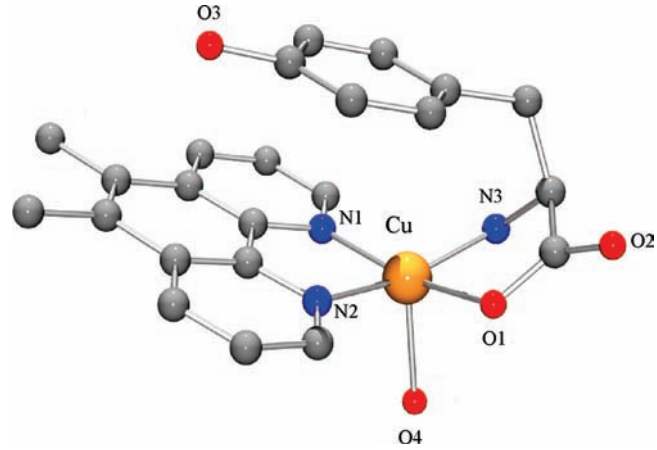

Figure 1. Ball-and-stick representation of the crystal structure of [Cu(L-tyr)(5,6-dmp)(H_2O)] (ClO_4) (**3**) showing atoms. Hydrogen atoms are omitted for clarity.

Table 1. Crystal Data and Structure Refinement Details of **3**

	3
empirical formula	C43 H35 Cl3 Cu2 N6 O21
fw	1205.22
cryst syst	orthorhombic
Space group	P212121
a, Å	7.5362(6)
b, Å	18.4379(14)
c, Å	35.228(3)
α, deg	90
β, deg	90
γ, deg	90
V, Å^3	4895.0(7)
Z	4
λ(Mo Kα), Å	0.71073
D_{calcd}, g·cm^{-3}	1.635
GOF on F^2	1.031
no. reflns measured	25289
no. reflns used	6382
no. refined params	399
Final R Indices [$I > 2\Sigma(I)$]	
R1[a]	0.0682
wR2[b]	0.1796[a]

[a] $R1 = [\Sigma(||F_o| - |F_c||)/\Sigma|F_o|]$. [b] $wR2 = \{[\Sigma(w(F_o^2 - F_c^2)^2)/\Sigma(wF_o^4)]^{1/2}\}$.

Description of the Crystal Structure of [Cu(L-tyr)(5,6-dmp)(H_2O)]ClO_4 (3). The ORTEP representation of the structure of complex **3** including the atom numbering scheme is shown in Figure 1, and the selected bond lengths and bond angles are listed in Tables 1 and 2, respectively. The asymmetric unit cell of **3** consists of two crystallographically independent molecules of the complex having essentially the same structure. The copper atom in each molecule is coordinated by the carboxylate oxygen (O1) and the amine

(24) Sigman, D. S. *Biochemistry* **1990**, *29*, 9098–9105.
(25) Uma Maheswari, P.; Palaniandavar, M. *Inorg. Chim. Acta* **2004**, *357*, 901–912.
(26) Bencini, A.; Berni, E.; Bianchi, A.; Giorgi, C.; Valtancoli, B.; Chand, D. K.; Schneider, H. J. *Dalton Trans* **2003**, *5*, 793–800.
(27) Mahadevan, S.; Palaniandavar, M. *Inorg. Chem.* **1998**, *37*, 3927–3934.
(28) Chikira, M.; Tomizava, Y.; Fukita, D.; Sugizaki, T.; Sugawara, N.; Yamazaki, T.; Sasano, A.; Shindo, S.; Palaniandavar, M.; Anthroline, W. E. *J. Inorg. Biochem.* **2002**, *89*, 163–173.
(29) Ramakrishnan, S.; Palaniandavar, M. *J. Chem. Sci.* **2005**, *117*, 179–186.
(30) Hirohama, Y.; Kuranuki, E.; Ebina, T.; Sugizaki, H.; Arii, M.; Chikira, P.; Tamil Selvi, P.; Palaniandavar, M. *J. Inorg. Biochem.* **2005**, *99*, 1205–1219.
(31) Hegg, E. L.; Burstyn, J. N. *Coord. Chem. Rev.* **1998**, *173*, 133–165.
(32) Mancin, F.; Scrimin, P.; Tecilla, P.; Tonellato, U. *Chem. Commun.* **2005**, 2540–2548.
(33) An, Y.; Liu, S.-D.; Deng, S.-Y.; Ji, L. N.; Mao, Z.-W. *J. Inorg. Biochem.* **2006**, *100*, 1586–1593.
(34) Jemal, A.; Thomas, A.; Murray, T.; Thun, M. *Cancer J. Clin.* **2002**, *52*, 23–47.
(35) Ferlay, J.; Bray, F.; Pisani, P. *GLOBOCAN 2000: Cancer Incidence, Mortality, and Prevalence Worldwide*, IARC Cancer Base No. 5; IARC Press: Lyon, France, 2001.
(36) (a) Sun, S.-Y.; Hail, N.; Lotan, R., Jr. *J. Natl. Cancer Inst.* **2004**, *96*, 662–672. (b) Thompson, C. B. *Science* **1995**, *267*, 1456–1462.
(37) Collins, J. G.; Sleeman, A. D.; Aldrich, J. R.; Greguric, I.; Hambly, T. W. *Inorg. Chem.* **1998**, *37*, 3133–3141.
(38) Addison, A. W.; Rao, T. N.; Reddijk, J.; van Rijn, J.; Veschoor, G. C. *J. Chem. Soc., Dalton Trans.* **1984**, 1349–1356.

Table 2. Selected Bond Lengths (Å) and Angles (deg) for **3**

	3
Bond Lengths (Å)	
Cu1−N1	2.006(5)
Cu1−N2	1.989(4)
Cu1−N3	1.994(5)
Cu1−O1	1.977(4)
Cu1−O4	2.244(4)
Angles (deg)	
O5 −Cu2 −O8	94.61(15)
O5 −Cu2 −N4	94.16(17)
O5−Cu2−N5	166.61(18)
O5−Cu2−N6	81.95(16)
O8−Cu2−N4	101.37(16)
O8−Cu2−N5	98.72(17)
O8−Cu2−N6	94.49(16)
N4−Cu2−N5	82.01(17)
N4−Cu2−N6	163.94(18)
N5−Cu2−N6	98.20(17)
O1−Cu1−N2	94.16(17)
O1−Cu1−N3	81.09(17)
O4−Cu1−N1	99.37(18)
O4−Cu1−N2	99.65(16)
O4−Cu1−N3	95.66(18)
O1−Cu1−O4	94.30(15)
O1−Cu1−N1	166.18(18)
N2−Cu1−N3	164.29(19)
N1−Cu1−N2	81.6(2)
N1−Cu1−N3	99.4(2)

nitrogen (N3) atoms of coordinated tyrosine anion, two nitrogen atoms (N1 and N2) of 5,6-dmp, and a water (O4) molecule. The value of the structural index[38] τ of 0.03 ($\tau = (\beta - \alpha)/60$, where α = N1 − Cu1 − O1 = 166.18° and β = N2 − Cu1 − N3 = 164.29°; for perfect square pyramidal and trigonal bipyramidal geometries, the τ values are zero and unity, respectively) reveals that the coordination geometry around copper(II) is best described as square pyramidal[39−41] with the corners of the CuN_3O basal plane being occupied by N1, N2, and N3 nitrogen and O1 oxygen atoms and the apical position being occupied by O4 oxygen atom. The $Cu-N_{amine}$ bond (Cu−N3, 1.994 Å) is almost the same in distance as the trans Cu−N1 (2.006 Å) and Cu−N2 (1.989 Å) bonds formed by the phen ring despite the expectation that the former should be longer than the $Cu-N_{phen}$ distances because of sp^3 and sp^2 hybridizations, respectively, of the amine and phen imine nitrogen atoms. The $Cu-N1_{phen}$ bond (2.006 Å) is slightly longer than the other $Cu-N2_{phen}$ bond (1.989 Å) because it is trans to the stronger Cu−O1 bond formed by the carboxylate group. The O4 atom is located apically at a distance of 2.244 Å, which is longer than the equatorial O1 atom (Cu−O1, 1.977 Å) as a consequence of the presence of two electrons in the d_{z^2} orbital. The complex exhibits intramolecular stacking between the side chain aromatic ring of the coordinated L-tyrosine and 5,6-dmp ligand with the former being located approximately parallel to the coordination plane.

Solution Structures. In Tris/HCl buffer solution, all complexes exhibit only one broadband in the visible region with very low absorptivity (Table S1 in the Supporting Information), which is consistent with the square-based geometry observed in the solid-state structure of **1**−**4**. The ESI-MS data reveal that the identities of the mixed ligand complex species are retained even in solution. The intense absorption band observed in the UV region (248−282 nm) is attributed to the intraligand $\pi \rightarrow \pi^*$ transitions due to the aromatic rings. The frozen solution EPR spectra are axial with $g_{\|} > g_{\perp} > 2.0$ and $G = [(g_{\|} - 2)/(g_{\perp} - 2)] = 3.6$, which suggests that the square-based geometries of the complexes observed in the solid state are retained in solution. Furthermore, a square-based CuN_4 chromophore is expected[42,43] to show a $g_{\|}$ value of 2.200 and an $A_{\|}$ value of (180−200) × 10^{-4} cm^{-1} (Table S1 in the Supporting Information), and the replacement of a nitrogen atom in this chromophore by an oxygen atom has been found to increase the $g_{\|}$ value and decrease the $A_{\|}$ value.[44] The incorporation of strong axial interaction, as in the present complexes, would increase the $g_{\|}$ and decrease the $A_{\|}$ values. Therefore, the observed values of $g_{\|}$ (2.257) and $A_{\|}$ ((170−180) × 10^{-4} cm^{-1}) for **1**−**4** are consistent with the presence of a square-based CuN_3O chromophore involving strong axial interaction, which is evident from the X-ray crystal structure of **3**.

DNA Binding Studies. Absorption Spectral Studies. Upon the addition of CT DNA to **1**−**4**, a decrease in the molar absorptivity (hypochromism, 34−49%, Figure S1 in the Supporting Information and Table 3) of the $\pi \rightarrow \pi^*$ absorption band with red shifts is observed, which indicates strong binding of the complexes to DNA. Because the extent of hypochromism is commonly associated with the strength of DNA interaction,[45−47] the observed order of decrease in hypochromism (Figure S2 in the Supporting Information), **4** > **3** > **2** > **1**, reflects the decreasing DNA binding affinities of the complexes in this order (cf. below). To enable quantitative comparison of the DNA binding affinities, we obtained the intrinsic binding constants, K_b, of the complexes for binding with calf thymus (CT DNA) by using the equation

$$[DNA]/(\varepsilon_a - \varepsilon_f) = [DNA]/(\varepsilon_b - \varepsilon_f) + 1/K_b(\varepsilon_b - \varepsilon_f)$$

where [DNA] is the concentration of DNA in base pairs, ε_a is the apparent extinction coefficient obtained by calculating A_{obs}/[complex], ε_f corresponds to the extinction coefficient of the complex in its free form, and ε_b refers to the extinction coefficient of the complex in the bound form. Each set of data, when fit to the above equation, gives a straight line with a slope of $1/(\varepsilon_b - \varepsilon_f)$ and a y intercept of $1/K_b(\varepsilon_b - \varepsilon_f)$,

(39) Murphy, G.; Nagle, P.; Murphy, B.; Hathway, B. *Dalton Trans.* **1997**, 2645–2652.
(40) Murphy, G.; Murphy, C.; Murphy, B.; Hathway, B. *Dalton Trans.* **1997**, 2653–2660.
(41) Nagle, P.; O'Sullivan, E.; Hathway, B. *J. Chem. Soc., Dalton Trans.* **1990**, 3399–3406.
(42) Tamil Selvi, P.; Murali, M.; Palaniandavar, M.; Kockerling, M.; Henkel, G. *Inorg. Chim. Acta B* **2002**, *340*, 139–146.
(43) Palaniandavar, M.; Somasundaram, I.; Lakshminarayanan, M.; Manohar, H. *Dalton Trans.* **1996**, 1333–1340.
(44) Murali, M.; Palaniandavar, M.; Pandiyan, T. *Inorg. Chim. Acta* **1994**, *224*, 19.
(45) Tysoe, S. A.; Morgan, R. J.; Baker, A. D.; Strekas, T. C. *J. Phys. Chem.* **1993**, *97*, 1707–1717.
(46) Kelly, J. M.; Tossi, A. B.; McConnell, D. J.; Strekas, T. C. *Nucleic Acids Res.* **1985**, *13*, 1707.
(47) Haworth, I. S.; Elcock, A. H.; Freemann, J.; Rodger, A.; Richards, W. G. J. *J. Biomol. Struct. Dyn.* **1991**, *9*, 23–43.
(48) Friedman, A. E.; Chamron, J. C.; Sauvage, J. P.; Turro, N. J.; Barton, J. K. *J. Am. Chem. Soc.* **1990**, *112*, 4960.

Table 3. Absorption Spectral Properties of Cu(II) Complexes Bound to CT DNA[a]

		ligand-based					
complex		λ_{max} (nm)	R	change in absorbance	$\Delta\varepsilon$ (%)	red shift (nm)	$K_b \times 10^3$ (M^{-1})
[Cu(L-tyr)(bpy)]$^+$	(**1**)	248	25	hypochromism	34	1	0.8 ± 0.10
[Cu(L-tyr)(phen)]$^+$	(**2**)	273	25	hypochromism	43	4	4.0 ± 0.08
[Cu(L-tyr)(5,6-dmp)]$^+$	(**3**)	282	25	hypochromism	44	0	6.5 ± 0.12
[Cu(L-tyr)(dpq)]$^+$	(**4**)	251	25	hypochromism	49	8	9.8 ± 0.16

[a] Measurements were made at $R = 25$, where R = [DNA]/[Cu complex]; concentration of copper(II) complex solutions = 2.0×10^{-5} M (**3**) and 3×10^{-5} M (**1**, **2**, and **4**).

and K_b was determined from the ratio of the slope to intercept. The intrinsic binding constants, K_b, obtained for the complexes follow the order **4** > **3** > **2** > **1**, suggesting that the diimine rather than the tyrosine "face" of the complexes is involved in DNA binding. Also, the observed range of K_b values ($(0.8 \times 10^3)-(0.98 \times 10^4)$ M^{-1}) is much lower than those observed for typical classical intercalators (EthBr, K_b, 1.4×10^6 M^{-1} in Tris−HCl/NaCl buffer (25:40 mM), pH 7.9) and partially intercalating metal[48] complexes ($[Ru(bipy)_2(dppz)]^{2+}$, dppz is dipyrido-[3,2-*d*:2′,3′-*f*]-phenazine, $K_b > 10^6$ M^{-1}) bound to CT DNA. Therefore, it is clear that the present monocationic complexes are involved in comparatively weak DNA binding interactions obviously due to the steric clash between the tyrosine ligand and DNA double helix. The coordinated dpq ring in **4** with larger aromatic ring surface area is engaged in partial insertion in between the base pairs of DNA much deeper than the coordinated phen ring in **2**, which leads to the higher DNA binding affinity of the former. This is consistent with the higher hypochromism (cf. above) and the higher red shift observed for **4** (**4**, 8; **2**, 4 nm). Interestingly, the red shifts observed are higher than those for the complexes[49] [Cu(imda)(phen)] (1 nm), [Cu(imda)(dpq)] (2 nm), and [Cu(imda)(5,6-dmp)] (0 nm), where H_2imda is iminodiacetic acid. It appears that the later complexes, because they are neutral, interact with DNA without affecting the energies of the ligand-based transitions very much. In this regard, we note that the partially DNA-intercalating dicationic complexes $[Ru(bpy)_2(diimine)]^{2+}$,[48] $[Ru(phen)_2(diimine)]^{2+}$,[50] $[Ru(5,6\text{-dmp})_2(diimine)]^{2+}$,[51,52] where diimine is phen, dpq, or dppz, and $[Ru(NH_3)_4(phen)]^{2+}$ [53] are known to exhibit significantly high red-shifts. Therefore, the present monocationic phen (**2**) and dpq (**4**) complexes show red shifts that are higher than the neutral [Cu(imda)(diimine)][49] complexes, which suggests their involvement in partial intercalative DNA interaction. The bpy complex **1** with only two nonplanar pyridine rings is obviously involved in weak binding to DNA. The introduction of methyl groups to the five and six positions of the phen ring, as in **3**, would be expected to hinder the partial intercalation of the phen ring, as evident from the zero red shift observed, and hence lead to a lower DNA binding affinity. However, the higher hypochromism and the higher K_b value obtained suggest that the DNA binding affinity of **3** is higher than that for the phen complex **2**. Therefore, it is proposed that the methyl groups on the phen ring of **3** are involved in hydrophobic interaction with the hydrophobic DNA surface leading to enhancement in DNA binding affinity. We previously observed similar enhanced DNA binding affinities for the complexes $[Ru(5,6\text{-dmp})(NH_3)_4]^{2+}$,[53] $[\{(5,6\text{-dmp})_2Ru\}_2(bpm)]^{4+}$,[54] [Cu(imda)(5,6-dmp)],[49] and $[Cu(dipica)(5,6\text{-dmp})]^{2+}$ [29] toward CT DNA. Therefore, the number of aromatic rings in the coligand and the modification of the phen ring dictate the DNA binding structure and affinity of the mixed ligand copper(II) complexes.

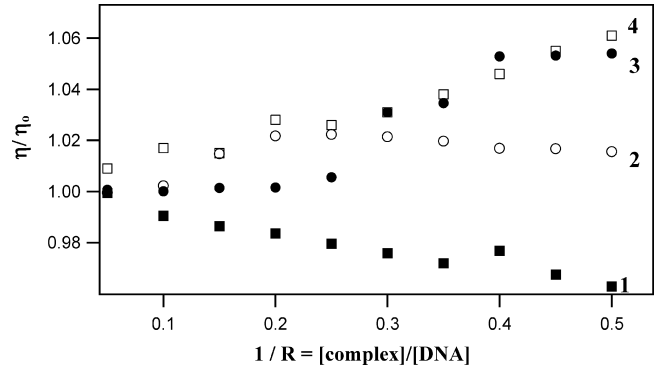

Figure 2. Effect of complexes **1**−**4** on the viscosity of CT DNA. Relative specific viscosity versus 1/*R*; [CT DNA] = 500 μM.

Viscosity Measurements. To understand the nature of DNA binding of the complexes, we carried out viscosity measurements on CT DNA by varying the concentration of added complexes. The values of relative specific viscosity (η/η_0), where η and η_0 are the specific viscosities of DNA in the presence and absence of the complex, are plotted against $1/R$ (= [Cu complex]/[NP] = 0.05 to 0.5) (Figure 2). The ability of the complexes to increase the viscosity of DNA depends on the diimine coligand: dpq (**4**) ≥ 5,6-dmp (**3**) > phen (**2**); negligible changes were observed for the bpy complex **1**, and this parallels the hypochromism and the K_b values (cf. above). The significant increase in viscosity of the dpq complex, which, however, is less than that for the potential intercalator viz., ethidium bromide,[55] is obviously due to the partial insertion of dpq ligand in between the DNA base pairs (cf. above), leading to an increase in the separation of base pairs at intercalation sites and, hence,

(49) Selvakumar, B.; Rajendiran, V.; Uma Maheswari, P.; Evans, H. S.; Palaniandavar, M. *J. Inorg. Biochem.* **2006**, *100*, 316–330.
(50) Dupureur, C. M.; Barton, J. K. *J. Am. Chem. Soc.* **1994**, *116*, 10286.
(51) Uma Maheswari, P.; Rajendiran, V.; Parthasarathi, R.; Subramanian, V.; Palaniandavar, M. *J. Inorg. Biochem.* **2006**, *100*, 3–17.
(52) Uma Maheswari, P.; Rajendiran, V.; Thomas, R.; Kulkarni, G. U.; Palaniandavar, M. *Inorg. Chim. Acta* **2006**, *359*, 4601–4612.
(53) Uma Maheswari, P.; Palaniandavar, M. *J. Inorg. Biochem.* **2004**, *98*, 219–230.
(54) Maheswari, P. U.; Rajendiran, V.; Parthasarathi, R.; Subramanian, V.; Palaniandavar, M. *Bull. Chem. Soc. Jpn.* **2005**, *78*, 835.
(55) Gabbay, E. J.; Scofield, R. E.; Baxter, C. S. *J. Am. Chem. Soc.* **1973**, *95*, 7850–7857.
(56) Baguley, B. C.; LeBret, M. *Biochemistry* **1984**, *23*, 937–943.

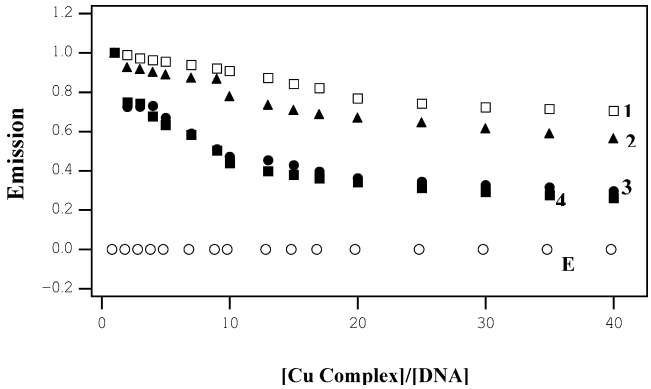

Figure 3. Effect of the addition of complexes **1**−**4** on the emission intensity of the CT DNA-bound ethidium bromide (125 μM) at different complex concentrations in a Tris−HCl buffer containing 5 mM Tris−HCl and 50 mM NaCl at pH 7.1 at 25 °C. E: addition of EthBr on CT DNA.

an increase in overall DNA contour length.[56] The lower lengthening of DNA duplex occurs for **2** upon the partial insertion of phen with fewer fused aromatic rings in between DNA base pairs. In contrast, a slight decrease in viscosity is observed for **1** because of kinking or bending of the DNA helices upon its binding. As discussed above, the presence of methyl groups on five and six positions of the phen ring would sterically hinder the partial insertion of the phen ring in between DNA base pairs, leading to no change in relative viscosity of DNA. But, interestingly, an increase in viscosity of DNA, as much as that for the dpq complex, is observed. It appears that the effective lengthening of the DNA duplex occurs on groove binding (see below) of the hydrophobically interacting 5,6-dmp complex. Similar observations have been made for other mixed ligand Cu(II) complexes of 5,6-dmp ligand. Therefore, viscosity studies confirm that the central ring of dpq and phen is involved in the partial intercalative mode of DNA binding, whereas the 5,6-dmp complex is involved in groove binding.

Ethidium Bromide Displacement Assay. In competitive ethidium bromide (EthBr) binding studies, complexes **1**−**4** have been added to DNA pretreated with EthBr ($1/R$ = [DNA]/[EthBr] = 40); then, the DNA-induced emission intensities of EthBr have been measured. It has been established[57] that free EB displays a decrease in emission intensity in Tris−HCl buffer medium because of quenching by solvent molecule. Therefore, if the complex binds DNA more strongly than EthBr, then the DNA-bound EthBr[58] would be displaced, leading to quenching of EthBr emission. The observed extent of decrease in emission intensity of EthBr **4** > **3** > **2** > **1** (Figure 3) is in conformity with the above order of DNA binding affinities. The higher reduction in emission intensity by **4** reveals that the presence of an extended aromatic planar ring such as dpq would facilitate the replacement of bound EthBr more than the other complexes. Interestingly, the 5,6-dmp complex, which is shown by viscosity and spectral measurements to be involved in groove binding but not intercalative binding, quenches the emission of DNA-bound EthBr more effectively than its phen analogue **2**. As expected, the bpy complex **1** shows the lowest DNA binding affinity, which implies that surface binding leads to the formation of kinks or bends in the DNA chain.

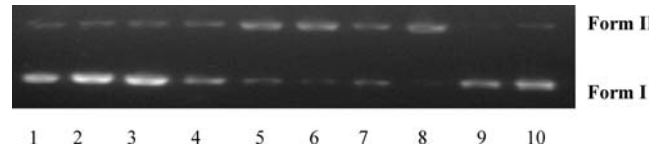

Figure 4. Cleavage of pUC19 supercoiled plasmid DNA (40 μM in base pair) without added reductant by the copper(II) complexes (100 μM) in a Tris−HCl buffer containing 5 mM Tris−HCl and 50 mM NaCl at pH 7.1 and 37 °C with an incubation time of 1 h. Lane 1, DNA; lane 2, DNA + [Cu(L-tyr)](ClO_4); lane 3, DNA +[Cu(L-tyr)$_2$]; lane 4, DNA + **1**; lane 5, DNA + **2**, lane 6, DNA + **3**, lane 7, DNA + **4**, lane 8, DNA + $[Cu(dpq)_2(H_2O)]^{2+}$; lane 9, DNA + $CuClO_4 \cdot 6H_2O$, lane 10, DNA + [Cu(5,6-dmp)$_2$Cl]Cl. Forms I and II are supercoiled and nicked circular forms of DNA, respectively.

Table 4. Self-Activated Cleavage Data of SC pUC19 DNA (40 μM in Base Pair) by Complexes **1**−**4** (0.1 mM) in the Absence of Any Reducing Agent for an Incubation Time of 1 h

		form %	
serial no.	reaction conditions	SC	NC
Figure A (0.1 mM Metal Concentration)			
1	DNA control	91.5	8.5
2	DNA + [Cu(L-Tyr)]$^+$	94.5	5.5
3	DNA + [Cu(L-Tyr)$_2$]	96.4	3.6
4	DNA + **1**	86.3	13.7
5	DNA + **2**	13.3	86.7
6	DNA + **3**	10.0	90.0
7	DNA + **4**	27.8	72.2
8	DNA + $[Cu(dpq)_2(H_2O)](ClO_4)_2$		100.0
9	DNA + $Cu(ClO_4)_2 \cdot 6H_2O$	93.4	6.6
10	DNA + [Cu(5,6-dmp)$_2$Cl]Cl	93.2	6.8

DNA Cleavage Studies. DNA Cleavage without Added Reductant. The copper(II) complexes **1**−**4** (100 μM) cleave double-stranded supercoiled plasmid pUC19 DNA (40 μM) (SC form; form I) into the nicked circular form (NC form; form II) at physiological pH 7.1 and temperature 37 °C in the absence of an activator. The mixed ligand complexes display cleavage activities more efficiently than do the corresponding mono- and bis-complexes of diimine coligand; interestingly, both mono- and bis(tyrosine)copper(II) complexes fail to cleave DNA. The DNA cleavage efficiency of the complexes follows the order **3** > **2** > **4** > **1**, depending on the diimine coligand at 100 μM concentration (Figure 4, Table 4). When the concentrations of **2**, **3**, and **4** are varied (10−200 μM) by keeping the DNA concentration (40 μM) constant, **4** exhibits efficient cleavage, even at 80 μM concentration, whereas **2** and **3** also show efficient cleavage but at 100 μM concentration. The mechanistic and kinetic aspects of **4**, which shows the most efficient DNA cleavage, are further studied. Under conditions of constant DNA concentration and varying complex concentration (10−160 μM) at the incubation period of 60 min, the k_{obs} values obtained increase but then decrease, which indicates that a pseudo Michaelis−Menten kinetic behavior is not followed (Figure S3 in the Supporting Information). When the maximum value of k_{obs} is set as V_{max}, the value of K_{cat} is calculated as 6.13 ± 1.00 h^{-1} under the present

(57) Waring, M. J. *J. Mol. Biol.* **1965**, *13*, 269.
(58) Lee, M.; Rhodes, A. L.; Wyatt, M. D.; Forrow, S.; Hartley, J. A. *Biochemistry* **1993**, *32*, 4237–4245.
(59) Dhar, S.; Reddy, P. A. N.; Chakravarty, A. R. *Dalton Trans.* **2004**, 697–698.

experimental conditions. The DNA cleavage has also been followed under true Michaelis-Menten kinetic conditions of constant catalyst concentration (80 μM) and varying substrate (Figure 5) concentration with an incubation period of 60 min. The higher rate constant calculated at 40 μM SC DNA (5.00 $\pm$ 0.1 h^{-1}) reveals that the complex cleaves DNA by about a million times faster than the uncatalyzed cleavage of double-stranded DNA. Also, the rate enhancement is significantly higher than that for the $[Cu(dpq)_2]^{2+}$ complex.[59] The extent of cleavage is found to vary exponentially with incubation time, and the cleavage follows pseudo-first-order kinetics. The kinetic plots show that the formation of NC form as well as the degradation of SC DNA versus time follow a pseudo-first-order kinetics and fit well into a single exponential curve at 0.8 mM (Figure 6A,B) complex concentration, and the plot of log (percent SC DNA) with time gives a linear fit.

The DNA strand scission chemistry of **4** has been further investigated by quantification of the supercoiled form. The distribution of supercoiled and nicked forms of DNA in the agarose gel electrophoresis provides a measure of the extent of hydrolysis of the phosphodiester bond. Although copper(II) complexes do not require an external agent like ascorbic acid, MPA, or H_2O_2 for cleavage, it has been noted that DNA cleavage occurs via a hydrolytic pathway. When the hydroxyl radical scavenger DMSO is added to the reaction mixture containing **4**, no inhibition of DNA cleavage is observed, which reveals that the cleavage reaction does not involve hydroxyl radicals (Figure S4 in the Supporting Information). Also, the extent of DNA cleavage under an argon atmosphere is found to be unaffected, suggesting that the cleavage pathway is oxygen independent. Furthermore, when the enzyme catalase is added as a coreactant in the cleavage reaction, no inhibition of cleavage is observed, which suggests the absence of involvement of H_2O_2 in the cleavage. Furthermore, the addition of excess of sodium chloride (250 mM) to the reaction mixture inhibits (but only slightly) the cleavage by **4** (Figure S4 in the Supporting Information), clearly indicating that the partial intercalation of coordinated dpq is important in enhancing the DNA

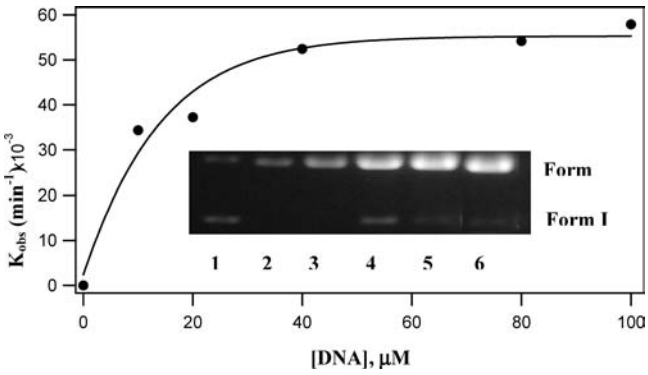

Figure 5. Concentration-dependent cleavage of pUC19 supercoiled plasmid DNA using 80 μM concentration of complex **4**. Various amounts of plasmid were reacted with a constant concentration of the complex for 1 h in a Tris−HCl buffer containing Tris−HCl/NaCl (5:50 mM) at pH 7.1 and 37 °C. Lane 1, pure supercoiled DNA 20 μM; lane 2, 20 μM DNA + 80 μM complex **4**; lane 3, 40 μM DNA + 80 μM complex **4**; lane 4, 80 μM DNA + 80 μM complex **4**; lane 5, 100 μM DNA + 80 μM complex **4**.

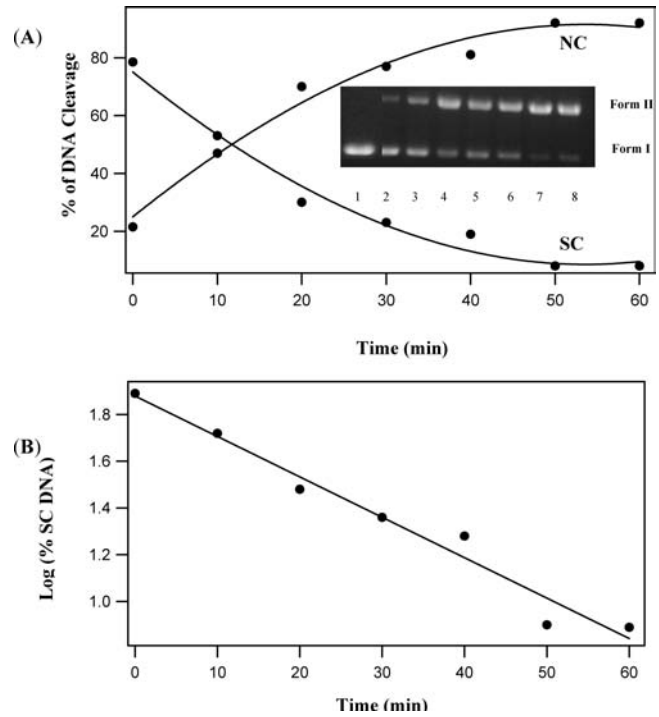

Figure 6. (A) Time course of pUC19 supercoiled plasmid DNA (40 μM in base pair) cleavage by complex **4** (80 μM) in a Tris−HCl buffer containing Tris−HCl/NaCl (5:50 mM) at pH 7.1 and 37 °C with incubation times of 0, 10, 20, 30, 40, 50, and 60 min for lanes 2−8, respectively. (B) Plot shows log (percent SC DNA) versus time for complex **4** (0.08 mM) at 37 °C (5 mM Tris−HCl and 50 mM at pH 7.1) for an incubation period of 0−60 min.

binding and cleavage. Furthermore, the addition of superoxide dismutase (superoxide scavenger) to the reaction mixture does not show significant quenching of the cleavage reaction, which reveals that superoxide anion is not also the active species.[60] To obtain further evidence of the mechanism of cleavage, we conducted additional cleavage experiments by using the T4 ligase enzymatic assay. When the linearized plasmid lambda/*Hin*dIII and pUC18/*Sau*3A−pUC18/*Taq*I digest was used as a positive control, the control was found to be religated. However, the present copper-mediated cleavage products were not religated under the same conditions (Figure S5 in the Supporting Information), suggesting that the DNA cleavage in the absence of added reductant does not involve a hydrolytic mechanism. We have previously observed a similar failure for $[Cu(tdp)(dpq)]^+$, where H(tdp) is 2-[(2-(2-hydroxyethylamino)-(ethylimino)methyl]phenol.[9] However, successful religation has been previously observed for certain other complexes.[61] It is possible that the hydrolytic cleavage products observed for **4** do not possess strictly matched ends suitable for religation; failure to religate does not mean the absence of hydrolytic DNA cleavage for **4**. Also, the dpq complex **4** shows a cleavage

(60) Gonalez-Alvarez, M.; Alzuet, G.; Borras, J.; Pitie, M.; Meunier, B. *J. Biol. Inorg. Chem.* **2003**, *8*, 644–652.
(61) Liu, C.; Yu, S.; Li, D.; Liao, Z.; Sun, X.; Xu, H. *Inorg. Chem.* **2002**, *41*, 913–922.
(62) (a) Thomas, A. M.; Nethaji, M.; Mahadevan, S.; Chakravarty, A. R. *J. Inorg. Biochem.* **2003**, *94*, 171–178. (b) Santra, B. K.; Reddy, P. A. N.; Neelakanta, G.; Mahadevan, S.; Nethaji, M.; Chakravarty, A. R. *J. Inorg. Biochem.* **2002**, *89*, 191–196.

activity lower than $[Cu(dpq)_2]^{2+}$, which has been reported[62] to cleave DNA to yield 100% NC but no LC form under conditions identical to the present one. In contrast, all other complexes show an order of cleavage higher than their corresponding bis-diimine complexes. Thus, the present study reveals that no diffusible radical is involved in the DNA cleavage observed in the absence of added reactant and that no dioxygen and H_2O_2 is needed for the cleavage.

DNA Cleavage with Added Reductant. The nuclease activity of the mixed ligand copper(II) complexes has been studied using supercoiled pUC19 DNA in Tris−HCl buffer containing NaCl in the presence of ascorbic acid as a reducing agent under dark conditions. All complexes convert supercoiled plasmid (SC) DNA into nicked circular (NC) DNA but not linear form. The control experiments performed by using **1**−**4** and ascorbic acid on separate lanes reveal no cleavage of DNA (Table S2 in the Supporting Information). The extent of DNA cleavage decreases in the order **4** (100%) > **2** (90.3%) > **3** (69.4%) > **1** (33.8%) depending upon the coligand (Figure S6 in the Supporting Information). Therefore, dpq complex **4** displays the highest DNA cleavage efficiency (100%), as much as $[Cu(dpq)_2]^{2+}$, which may be related to the ability of the dpq coligand with extended aromatic ring to engage in strong partial intercalative binding with DNA. As discussed above, the phen ring in **2** is involved in weaker partial intercalation between the DNA base pairs. Whereas the lower DNA cleavage activity of the 5,6-dmp complex is consistent with its DNA groove binding, the lowest nuclease activity of the bpy (**1**) complex reveals its DNA binding on its surface. So it is obvious that partial intercalation is important for an efficient DNA cleavage activity and that the DNA groove-bound 5,6-dmp complex does not expose the 5,6-dmp ring, unlike **2** and **4**, close to ribose C1−H bond for H-abstraction. The preliminary mechanism of pUC19 DNA cleavage by **1**−**4** has been studied by using different inhibitors/scavengers. When the hydroxyl radical inhibitor DMSO is added to the reaction mixture (Figure S7 in the Supporting Information), a significant decrease in nuclease activity is observed, which indicates the involvement of the hydroxyl radical in the cleavage process. The Cu(II) complex−DNA adduct formed would undergo reduction by the added reductant to form the Cu(I) complex−DNA adduct, which then generates hydroxyl radicals or activated oxygen species by reaction with $^3O_2$. The hydroxyl radicals attack the DNA to cause strand scission. When the minor groove binder distamycin (Figure S8 in the Supporting Information) is added to the reaction mixture containing **4**, the DNA cleavage is inhibited, revealing the binding of the dpq complex in the DNA minor groove.[63]

Photoinduced DNA Cleavage Studies. We studied photoinduced DNA cleavage activities of **1**−**4** at 25 μM concentration by using SC plasmid pUC19 DNA in Tris−HCl/NaCl (5:50 mM) buffer at pH 7.1 and irradiating with UV light at 365 nm (Figure S9 and Table S3 in the Supporting Information). All complexes displayed a small extent of DNA cleavage, but **4** showed a higher order of DNA cleavage under experimental conditions similar to that of its bis-complex $[Cu(dpq)_2(H_2O)](ClO_4)_2$. Control experiments indicated that the ligands L-tyrosine and dpq and $Cu(ClO_4)_2 \cdot 6H_2O$ failed to show DNA cleavage at 365 nm irradiation. When a singlet oxygen quencher such as sodium azide[60] was added to the reaction mixture containing **4**, no inhibition of DNA cleavage activity was noted. When D_2O, in which singlet oxygen has a longer lifetime was used as solvent, no significant change in cleavage was observed. Both of these observations rule out the involvement of singlet oxygen in the photoinduced DNA cleavage reactions. When SOD was added to the reaction mixture, it did not have an apparent effect on the cleavage activity, indicating the noninvolvement of O_2^- in the cleavage reaction. Furthermore, the addition of the hydroxyl radical scavenger DMSO to the reaction mixture tended to inhibit the cleavage reaction, suggesting involvement of hydroxyl radicals in the photocleavage reaction[9] (Figure S10 in the Supporting Information).

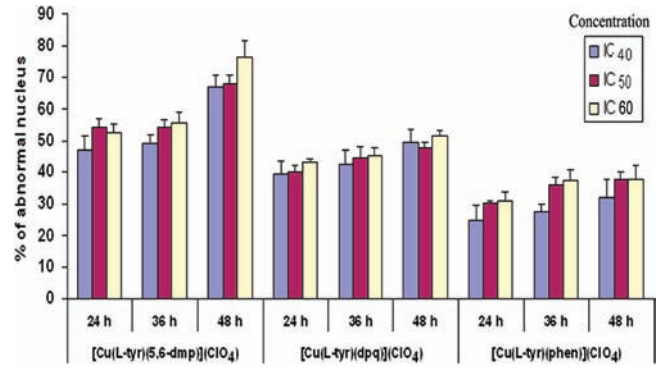

Figure 7. Data showing counts of cells with normal and abnormal nuclear features. Abnormal cells increase in a time-dependent manner for **2**−**4**. Data are mean values obtained from two independent experiments, and bars represent standard deviations.

Table 5. In Vitro Cytotoxicity Assays for Complexes **2**−**4** against H-460 Lung Cancer Cell Line

complexes	IC_{50} value (nM)	
	24 h	48 h
Cu(L-tyr)(phen)](ClO4) **2**	<5000	3400 ± 175
$[Cu(L\text{-tyr})(5,6\text{-dmp})](ClO_4)$ **3**	2400 ± 150	900 ± 230
$[Cu(L\text{-tyr})(dpq)](ClO_4)$ **4**	4700 ± 210	2400 ± 75

Anticancer Activity Studies. The anticancer activities of the strongly DNA binding complexes **2**−**4** toward human nonsmall lung cancer cell line (NCI-H460) have been examined in comparison with the currently used drug cisplatin under identical conditions by using MTT assay. It is found that the complexes exhibit significant cytotoxic activities (IC_{50}, 900−4900 nM, Figure 7 and Table 5) in a time-dependent manner. Whereas **2** and **4** exhibit appreciable cytotoxic effects with IC_{50} values varying in a comparatively narrow range, **3** is remarkable in displaying the most prominent cytotoxicity (IC_{50}, 900 nM after

(63) Ferrer, S.; Bellesteros, R.; Sambartolome, A.; Gonazalez, M.; Alzuet, G.; Borras, J.; Liu, M. *J. Inorg. Biochem.* **2004**, *98*, 1436–1446.
(64) Kalinowska-Lis, U.; Ochocki, J.; Matlawska-Wasowska, K. *Coord. Chem. Rev.* **2008**, *252*, 1328–1345.

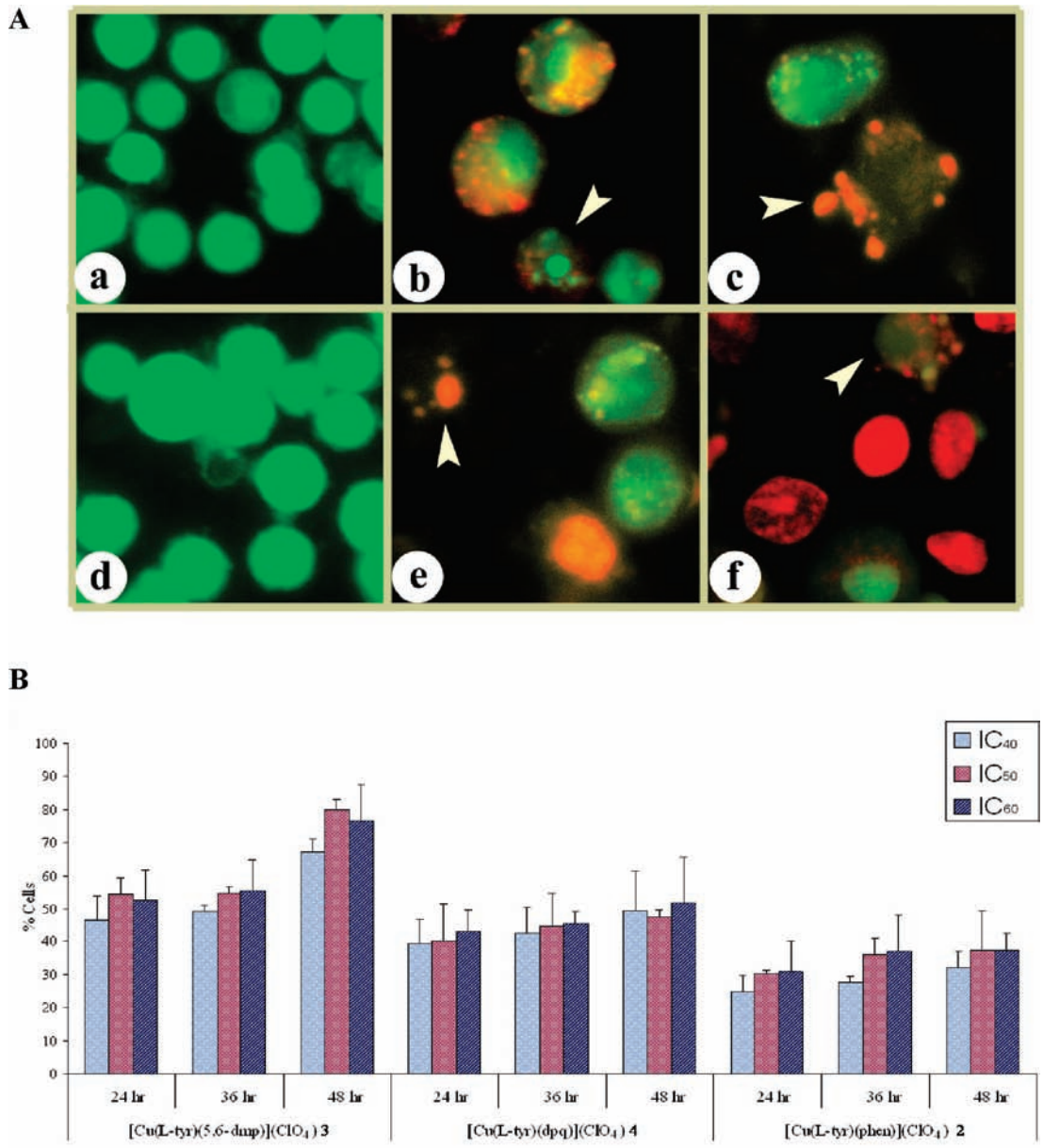

Figure 8. (A) AO/EB-stained H-460 lung cancer cells. (a,d) Untreated cells (green), (b,c) treatment of complex **3**, and (e,f) complex **4** at 24 and 48 h of incubation. (B) AO/EB fluorescent study of **2**−**4**-induced apoptosis of NCI-H460 cells. Graph shows manual count of apoptotic cells in percentage. (Data are mean percent ± SD percent of triplicate each).

48 h) with its activity equal to cisplatin.[64] Apoptosis is a naturally occurring gene-controlled process that plays a critical role in tissue homeostasis and elimination of unwanted cells in animals without affecting normal/unaffected cells. Most tumor cells still remain sensitive to some apoptotic stimuli from chemotherapeutic agents, and in this context, the apoptosis-inducing ability of drugs seems to be a primary factor in determining their efficacy.[65] Therefore, we have studied the mode of cell death induced by **2**−**4** by adopting fluorescent staining for morphological assessment of cell death, single cell gel electrophoresis (comet assay) for detecting DNA fragmentation, and flow cytometry for DNA content analysis of the treated cells against control cells.

The characteristic morphological changes brought about in the cells by treatment with complexes **2**−**4** have been evaluated by adopting fluorescent microscopic analysis of Hoechst 33258- and AO/EB-stained cells. The results obtained indicate that the complexes induce cell death through different modes like mitotic catastrophe, necrosis, and apoptosis. After treating the cells with IC_{40}, IC_{50}, or IC_{60} concentrations of the complexes at different time intervals (24, 36, and 48 h) we have observed cytological changes such as chromatin fragmentation, bi- and multinucleation, cytoplasmic vacuolation, nuclear swelling, cytoplasmic blebbing, and late apoptosis indication of dotlike chromatin condensation (Figure S11 in the Supporting Information) by adopting Hoechst 33258 staining. The cytological changes

(65) Ghobrial, I. M.; Witzig, T. E.; Adjei, A. A. *Cancer J. Clin.* **2005**, *55*, 178.
(66) Sihn, C. R.; Suh, E. J.; Lee, K. H.; Kim, T. Y.; Kim, S. H. *Cancer Lett.* **2003**, *201*, 203–210.

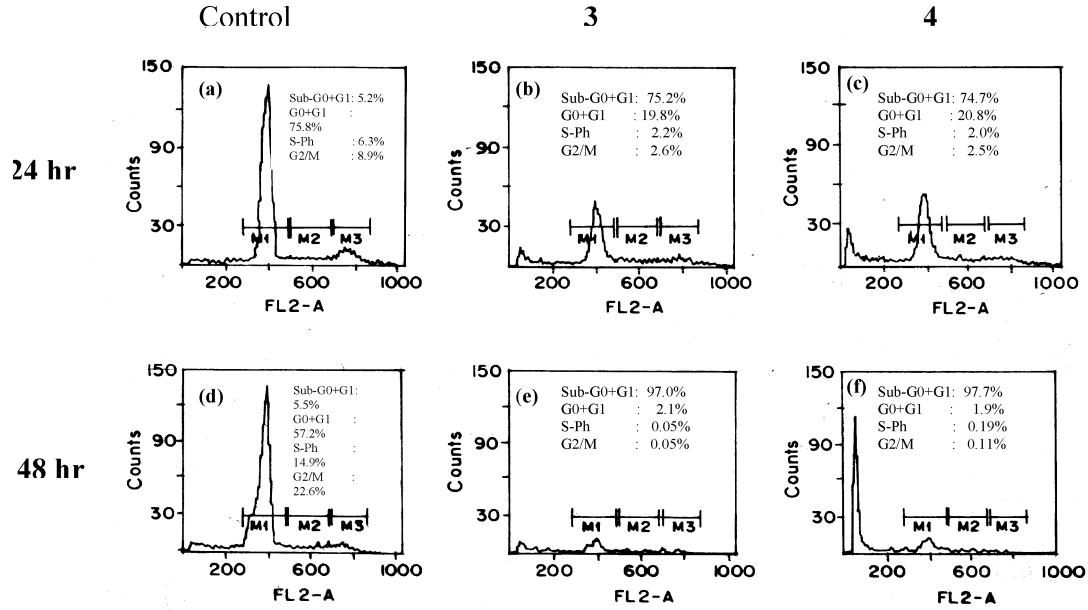

Figure 9. Effect of complexes **3** and **4** on the distribution of H-460 cells in cell cycle progression. The cell cycle phase was determined by the cellular DNA content measured by flow cytometry of PI-stained cells. G_1, S, and G_2/M denote the corresponding phases of the cell cycle. Sub-G_1 events correspond to cells or cell fragments with lower DNA content and are indicative of the apoptotic death of the cells. Cell cycle distribution is shown as histograms. Untreated cells are used as controls for **3** and **4** (a: 24 h and d: 8 h). Cells are treated with **3** (b: 24 h and e: 48 h) and **4** (c: 24 h and f: 48 h).

observed are generally classified into four types according to the fluorescence emission and morphological features of chromatin condensation in the AO/EB stained nuclei: (i) viable cells that have uniformly green fluorescing nuclei with highly organized structure; (ii) early apoptotic cells (which still have intact membranes but have started undergoing DNA fragmentation) that have green fluorescing nuclei but where perinuclear chromatin condensation is visible as bright green patches or fragments; (iii) late apoptotic cells that have orange to red fluorescing nuclei with condensed or fragmented chromatin; and (iv) necrotic cells, swollen to large sizes, that have uniformly orange to red fluorescing nuclei with no indication of chromatin fragmentation. All of these morphological changes are observed for **2**−**4**, suggesting that the cells are committed to death in such a way that both apoptotic and necrotic cells increase in number in a time-dependent manner. The apoptotic morphologies induced by the complexes are confirmed by AO/EB staining adopting fluorescence microscopy, which reveals the apoptotic cell death from the perspective of fluorescence (Figure 8A). All of these results suggest that the complex **3** causes more cells to take to one particular mode of cell death preferentially during 48 h of treatment than during 24 h of treatment. Similar observations are also made for **2** and **4**, and the changes are time-dependent, but the respective percentages of cell death are comparatively less (Figure 8B).

To investigate the mechanism of cell division and cell death induced by **3** and **4** on H-460 cells, we employed the fluorescence-activated cell sorting (FACS) analysis of the DNA content. The cells were treated with the complexes, the cell cycle progression was analyzed at different incubation times (24, 48 h), and the results are presented (Figure 9). In the control experiments, 5.2 and 5.5% of the cells were found to be populated at sub-G_0/G_1 (apoptotic) phase for the incubation periods of 24 and 48 h, respectively, and also, higher percentages of cells were populated at the G_0/G_1 phase (75.8% at 24 h; 57.4% at 48 h) and lower percentages of cells were populated at the S phase and G_2/M phases. It is well known that in this analysis, the cells in the G_0/G_1 phase have unreplicated diploid (2n) DNA content, whereas the G_2/M phase has replicated ploid (4n) DNA. Also, hypodiploidy (<2n) DNA content at the sub-G_0/G_1 phase and replication in the S phase are observable. Upon exposure of the cells to **4**, the accumulation of cells increased in the sub-G_0/G_1 phase from 5.2 (control) to 74.7% at 24 h and from 5.5 (control) to 97.7% at 48 h, and thus the percentage of cells accumulated at this phase increased with incubation time. Also, the percentages of cells decreased in the remaining phases of the cell cycle (G_0/G_1, 19.8 to 2.1%; S, 2.2 to 0.5%; G_2/M, 2.6 to 0.5%) with incubation time, indicating blockage of cell progression into G_0/G_1, S, and G_2/M phases and hence inhibition of DNA replication.[66] All of these observations reveal that the major mode of cell death induced by **4** is apoptosis because the accumulation of hypodiploid cells in the sub-G_0/G_1 phase is considered[67−69] to be a marker for apoptotic cell death. Several intracellular cascades such as activation of caspases, disruption of normal mitochondrial function, or both would be involved in the road map toward the final destination, that is, the apoptotic cell death.[70]

(67) Heffeter, P.; Jakupec, M. A.; Ḱ orner, W.; Wild, S.; Von Keyserlingk, N. G.; Elbling, L.; Zorbas, H.; Koryneuska, A.; Knasm̈ uller, S.; Sutterl ̈ uty, H.; Micksche, M.; Keppler, B. K.; Berger, W. *Biochem. Pharmacol.* **2006**, *71*, 426.
(68) Sprenger, C. C.; Vail, M. E.; Simurdak, J.; Plymate, S. R. *Oncogene* **2000**, *21*, 140.
(69) Wang, T.-C.; Chen, L.-L.; Lu, P.-J.; Wong, C.-H.; Liao, C.-H.; Tsiao, K.-C.; Chang, K.-M.; Chen, Y.-L.; Tzeng, C.-C. *Bioorg. Med. Chem.* **2005**, *13*, 6045.
(70) Singh, N. P.; McCoy, M. T.; Tice, R. R.; Schneider, E. L. *Exp. Cell Res.* **1988**, *175*, 184.

In contrast with **4**, complex **3** brings about fragmentation of H-460 cells with lower DNA content and maximum disappearance of all phases at 48 h (Figure 9). It is possible that cells have entered into the hypoploid level, hyperploid level (>4n), or both beyond the G_2/M phase possibly due to the formation of multiple micronuclei in the absence of cytokinesis. Such an observation corresponds to the death of cells through mitotic catastrophe,[71] a mode different from the apoptosis mode of cell death induced by **4**. However, it has been suggested[72,73] more recently that mitotic catastrophe should be regarded as an abnormal mitosis that leads to cell death rather than an actual form of cell death, which can occur through necrosis or apoptosis. In this regard, it may be noted that apoptotic morphological features have been observed for **3** (cf. above).

DNA fragmentation is a hallmark of apoptosis, mitotic catastrophe, or both and is detected at a single cell level by the use of single cell gel electrophoresis (comet) in agarose gel matrix. When a cell with damaged DNA is subjected to electrophoresis and then stained with ethidium bromide (EthBr), it appears as a comet, and the length of the comet tail represents the extent of DNA damage.[74] Cells treated with **3** and **4** show statistically significant well-formed comets, whereas the control (untreated) cells do not demonstrate any cometlike appearance (Figure 10). Also, the tail length observed for **3** is longer than that for **4**, which is consistent with the higher cytotoxicity observed for **3** (cf. above). This clearly indicates that both of the complexes indeed induce DNA fragmentation, which is further evidence of apoptosis. The DNA fragmentation induced by the complexes is confirmed by DNA laddering assay. The degradation of DNA into oligonucleosomal fragments of 150−200 bp is a distinct biochemical hallmark of apoptosis. The control cells do not show any band(s) in the 150−200 base pair region, whereas cells treated with **4** result in a prominent band appearing in the 150−200 base pair region (Figure S12 in the Supporting Information), which reveals the involvement of DNA fragmentation in cell death. This is consistent with the cytological changes in cell morphology and apoptosis[75] that are observed for **4** (vide supra). However, no such DNA ladder formation is observed for **3**, and this is expected[76] because cells undergoing mitotic catastrophe usually fail to show DNA ladder formation.

The results of MTT assay and comet assay and the morphological changes observed, along with the absence of DNA ladder formation, reveal that complex **3** possesses a very prominent cytotoxicity, which is consistent with its strong DNA binding involving hydrophobic forces of interaction and efficient DNA cleavage. It is interesting to note that the mixed ligand complex $[Cu(tdp)(tmp)]^+$, where tmp is 3,4,7,8-tetramethyl-1,10-phenanthroline, also exhibits a stronger DNA binding through hydrophobic forces of interaction and shows[9] a higher percentage of apoptotic cell death than that of the other $[Cu(tdp)(diimine)]^+$ complexes. Therefore, it appears that the higher cytotoxicity of **3** may originate from the combined effect of the hydrophobic 5,6-dmp ligands and the hydrophilic L-tyrosine with a phenolic hydroxyl group in the complex, which facilitates its transport into the cell across the cell membrane and its eventual release at the various organelles in the cell, which leads to mitotic catastrophe. Also, it is possible that hydrophobic complex **3** might bind very strongly to the cellular proteins that controlling mitosis and deplete them, thus contributing to the abnormal nuclear division and subsequent cell death.[9,76] Interestingly, the percentages of dead cells observed for **4** at the apoptotic phase at low incubation time are higher than those observed[9] for the mixed ligand complexes $[Cu(tdp)(diimine)]^+$, revealing that **4** is more potent than the latter in inducing apoptosis. It is obvious that the induction of cell death by **4** might be associated with DNA damage, as inferred from the cleavage of plasmid DNA by **4** (Figure 3 in the Supporting Information). Also, the different modes of cell death induced by **3** and **4** might originate from the differences in their DNA binding modes and DNA cleavage efficiencies (cf. above) and thus throw light on the interesting roles of the coligands. We note that the dpq complex **4** is more efficient than the 5,6-dmp complex **3** toward DNA binding and DNA cleavage at low complex concentrations (cf. above). Furthermore, the transport of the dpq complex into the cell across the cell membrane is expected to be less facile than that of the hydrophobic 5,6-dmp complex. However, complex **4**

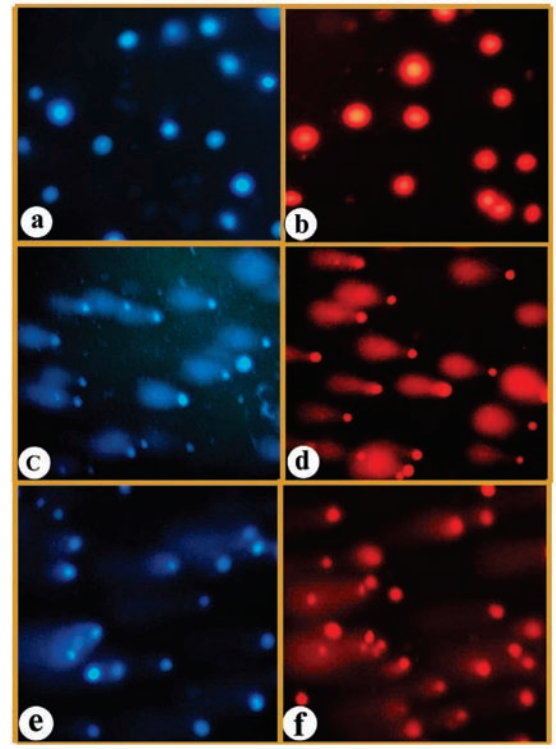

Figure 10. Comet assay of (a) Hoechst-33258-dye stained and (b) EB-stained control (untreated) H-460 cells and (c,d) **3** and (e,f) **4** treated cells.

(71) Eom, Y.-W.; Kim, M. A.; Park, S. S.; Goo, M. J.; Kwon, H. J.; Sohn, S.; Kim, W.-H.; Yoon, G.; Choi, K. S. *Oncogene* **2005**, *24*, 4765–4777.
(72) Chu, K.; Teele, N.; Dewey, M. W.; Albright, N.; Dewey, W. C. *Radiat. Res.* **2004**, *162*, 270–286.
(73) Nitta, M.; Kobayashi, O.; Honda, S.; Hirota, T.; Kuninaka, S.; Marumoto, T.; Ushio, Y.; Saya, H. *Oncogene* **2004**, *23*, 6548–6558.
(74) Alapetite, C.; Wachter, T.; Sage, E.; Moustacchi, E. *Int. J. Radiat. Biol.* **1996**, *69*, 359.
(75) (a) Kaufmann, S. H. *Cancer. Res.* **1989**, *15*, 5870–5878. (b) Distelhorst, C. W. *Blood* **1988**, *72*, 1305–1309.
(76) He, Q. Y.; Liang, Y. Y.; Wang, D. S.; Li, D. D. *Int. J. Oncol.* **2002**, *20*, 261–266.

appears to be more efficacious than **3** because it exhibits apoptosis-inducing ability, which is a critical factor in determining its efficacy.[65]

Conclusions

The mixed ligand copper(II) complexes of the type [Cu(L-tyr)(diimine)](ClO_4), where L-tyr is the amino acid L-tyrosine and diimine is 2,2′-bipyridine (bpy), 1,10-phenanthroline (phen), 5,6-dimethyl-1,10-phenanthroline (5,6-dmp), or dipyridoquinoxaline (dpq), have been isolated. The single crystal X-ray structure of [Cu(L-tyr)(5,6-dmp)(H_2O)](ClO_4) has been determined, and an almost perfect square pyramidal structure is revealed. The square-based geometries of the complexes are preserved in aqueous buffer solution as diagnosed by ligand-field and axial EPR spectra. The phen and dpq complexes are involved in partial intercalative interaction of the phen and dpq rings with DNA, whereas the 5,6-dmp complex is involved in hydrophobic interaction of its methyl groups with DNA surface. The bpy complex is involved in electrostatic interaction with the exterior phosphates of DNA.

Interestingly, the dpq complex shows a profound efficiency to cleave plasmid DNA oxidatively, which is higher than those by the analogous mixed ligand bpy, phen, and 5,6-dmp complexes and the $[Cu(dpq)_2]^{2+}$ complex as well. Also, the cleavage studies reveal that the bpy, phen, and dpq complexes are bound in the DNA minor groove, whereas the 5,6-dmp complex is preferentially docked in the DNA major groove. It is remarkable that all four complexes are also effective in promoting cleavage of plasmid DNA, with the phen and 5,6-dmp complexes cleaving DNA faster than the dpq complex at higher concentrations. However, the dpq complex shows a fully efficient DNA cleavage at a minimum concentration of 80 μM, but there is a decrease in cleavage at higher concentrations. The carboxylate group of the amino acid, a water molecule present in the axial copper site, or both could be responsible for promoting cleavage of DNA, with the diimine being used as a DNA recognition element for DNA binding. The high rate of DNA hydrolysis of 5.00 ± 0.1 h^{-1} observed for the dpq complex provides information that is useful in designing copper(II) complexes as synthetic nucleases. Also, the observation of both the oxidative DNA cleavage with added chemical reagent and 365 nm light and DNA cleavage reveals the unique ability of the mixed ligand dpq complex to bring about DNA double-strand cleavage. Therefore, the present study proposes the dpq complex as a new and better DNA-binding and DNA-cleaving agent and, hence, as an artificial restriction enzyme in nucleic acid chemistry.

Interestingly, the phen, 5,6-dmp and dpq complexes exhibit anticancer activities that are more-or-less equivalent to the widely used drug cisplatin, which is consistent with the results from DNA binding and cleavage studies. The comet assay, DNA fragmentation assay, and cell cycle analysis clearly indicate that both the 5,6-dmp and dpq complexes would act as potent antiproliferative agents by inducing morphological changes consistent with the induction of mitotic catastrophe and apoptotic cell death, respectively. To the best of our knowledge, the 5,6-dmp complex is the first copper(II) complex reported so far to exhibit a mitotic catastrophe mode of cell death. Additionally, we have shown that the dpq complex can induce specific DNA fragmentation and hypodiploid pattern in DNA content, which are hallmarks of apoptosis, and thus can act as an efficacious anticancer agent. Further studies are needed to prove the role of regulatory proteins associated with cell division and apoptosis, which would elucidate the identification of additional molecular targets for the development of potent transition-metal-based chemotherapeutic agents.

Experimental Section

Reagents and Materials. Copper(II) perchlorate hexahydrate (Aldrich), 1,10-phenanthroline and L-tyrosine (Merck), calf thymus (CT) DNA (highly polymerized stored at 4 °C), superoxide dismutase (SOD), catalase (Sigma, stored at −20 °C), pUC19 supercoiled plasmid DNA, and agarose (Genei, Bangalore, India) were used as received. Ultrapure Milli-Q water (18.2 mΩ) was used in all experiments. The ligand dipyrido-[3,2-*d*:2′,3′-*f*]-quinoxaline (dpq) was prepared by the reported procedure.[37] The commercial solvents were distilled and were then used for the preparation of complexes.

Cell Culture. The NCI-H460 human lung cancer cell line was obtained from the National Center for Cell Science (NCCS), Pune, India. The cells were cultured in RPMI 1640 medium (Biochrom AG, Berlin, Germany) supplemented with 10% fetal bovine serum (Sigma), cisplatin (Getwell pharmaceuticals, India), mitomycin C (Sigma) and 100 U/mL penicillin and 100 μg/mL streptomycin as antibiotics (Himedia, Mumbai, India) in 96-well culture plates at 37 °C under a humidified atmosphere of 5% CO_2 in a CO_2 incubator (Heraeus, Hanau, Germany). All experiments were performed using cells from passage 15 or less.

Methods and Instrumentation. Microanalyses (C, H, and N) were carried out with a Vario EL elemental analyzer. An LCQ DECA XP electrospray mass spectrometer was employed for ESI-MS analysis. UV−vis spectroscopy was recorded on a Varian Cary 300 Bio UV−vis spectrophotometer using cuvettes of 1 cm path length. Electron paramagnetic resonance (EPR) spectra of the mixed ligand complexes were obtained on a Varian E 112 EPR spectrometer. The spectra were recorded for solutions of the compound in DMF at liquid nitrogen temperature (LNT). DPPH was used as the field marker. Emission intensity measurements were carried out using a Jasco F 6500 spectrofluorimeter. Circular dichroic spectra of DNA were obtained by using a JASCO J-716 spectropolarimeter equipped with a peltier temperature control device. Viscosity measurements were carried out using a Schott Gerate AVS 310 automated viscometer.

Solutions of DNA in the buffer NaCl/Tris HCl (50:5 mM) in water gave the ratio of UV absorbance at 260 and 280 nm, A_{260}/A_{280}, as 1.9,[77] indicating that the DNA was sufficiently free of protein. Concentrated stock solutions of DNA (13.5 mM) were prepared in buffer and sonicated for 25 cycles, where each cycle consisted of 30 s with 1 min intervals. The concentration of DNA in nucleotide phosphate (NP) was determined by UV absorbance at 260 nm after 1:100 dilutions. The extinction coefficient, ε_{260}, was taken as 6600 $M^{-1}\cdot cm^{-1}$. Stock solutions were stored at 4 °C and used after no more than 4 days. Supercoiled plasmid pUC19 DNA was stored at −20 °C, and the concentration of DNA in base pairs was determined by UV absorbance at 260 nm after appropriate dilutions taking ε_{260} to be 131 00 $M^{-1}\cdot cm^{-1}$. We prepared concentrated stock solutions of metal complexes by dissolving

(77) Murmur, J. *J. Mol. Biol.* **1961**, *3*, 208.

calculated amounts of metal complexes in respective amounts of solvent, and they were suitably diluted with corresponding buffer to required concentrations for all experiments.

Preparation of Copper(II) Complexes. [Cu(L-tyr)(bpy)(H_2O)]ClO_4: ESI-MS: $[Cu(L\text{-}tyr)(bpy)]^+$ displays a peak at *m/z* 399.07 (399.07 calcd). [Cu(L-tyr)(phen)(H_2O)]ClO_4: ESI-MS: $[Cu(L\text{-}tyr)(phen)]^+$ displays a peak at *m/z* 422.93 (calcd 423.07) The complexes were prepared by the use of the published procedures.[78]

Caution! *During handling of the perchlorate salts of metal complexes with organic ligands, care should be taken because of explosion.*

[Cu(L-tyr)(5,6-dmp)(H_2O)](ClO_4) (3). We prepared this complex by adding a mixture of L-tyrosine (0.181 g, 1 mM), which was deprotonated by NaOH (1 mmol equivalent) in water and 5,6-dimethyl-1,10-phenanthroline (0.208 g, 1 mM) in methanol to a methanolic solution of copper(II) perchlorate (0.370 g, 1 mM) solution and then stirring the solution at 80 °C for 2 h for dissolution. The resulting solution was filtered and kept aside for crystallization by slow evaporation at room temperature. The blue crystalline solid separated out was collected by suction filtration, washed with small amounts of cold methanol, and dried in vacuum. When the concentrated solution was kept a week, blue colored crystals suitable for X-ray diffraction were obtained. Anal. Calcd: C, 48.51; H, 4.25; N, 7.38. Found: C, 48.52; H, 4.23; N, 7.37. ESI-MS: $[Cu(L\text{-}tyr)(5,6\text{-}dmp)]^+$ displays a peak at *m/z* 451.20 (calcd 451.11).

[Cu(L-tyr)(dpq)(H_2O)](ClO_4) (4). We prepared this complex by adding a methanol/water (4:1 v/v) solution of dpq (0.282 g, 1 mM) and a solution of L-tyrosine (0.133 g, 1mmol), which was deprotonated by adding an equimolar solution of NaOH, to an aqueous methanol solution of copper(II) perchlorate (0.37 g, 1 mM) and then stirring at 80 °C for 1 h. The resulting solution was filtered and set aside for crystallization by slow evaporation at room temperature. The blue crystalline solid separated out was collected by suction filtration, washed with small amounts of cold methanol, and dried in vacuum. Anal. Calcd: C, 46.55; H, 3.40; N, 11.80. Found: C, 46.54; H, 3.39; N, 11.82. ESI-MS: $[Cu(L\text{-}tyr)(dpq)]^+$ displays a peak at *m/z* 475.13 (calcd 475.08).

X-ray Crystallography. Crystal data were collected on an Enraf Nonius MACH2 diffractometer equipped with graphite-monochromated Mo Kα radiation ($\lambda = 0.71073$ Å). Data were corrected for Lorentz and polarization effects. The structures were solved with SIR-92 and refined with the SHELXL-97[79] package incorporated in WINGX 1.64 crystallographic collective package. Anisotropic refinements were performed by a full-matrix least-squares procedure on F^2. The positions of the hydrogen atoms were calculated assuming ideal geometries but not refined. Crystal data, data collection, and refinement parameters for **3** are listed in Table 1.

DNA Binding and Cleavage Experiments. We prepared concentrated stock solutions of metal complexes by dissolving them in Tris−HCl/NaCl (5:50 mM) buffer at pH 7.1 and suitably diluting them with the corresponding buffer to required concentrations for all experiments. For absorption and emission spectral experiments, the DNA solutions were pretreated with solutions of metal complexes to ensure no change in the concentration of the metal complexes.

We performed absorption spectral titration experiments on a Varian Cary 300 Bio UV−vis spectrophotometer by maintaining a constant concentration of the complex while varying the nucleic acid concentration. This was achieved by dissolving an appropriate amount of the complex and DNA stock solutions while maintaining the total volume constant (1 mL). This resulted in a series of solutions with varying concentrations of DNA but with a constant concentration of the complex. The absorbance (*A*) of the most red-shifted band of each investigated complex was recorded after successive additions of CT DNA pretreated with the complex.

The cleavage of DNA in the absence of activating agents was monitored using agarose gel electrophoresis. In cleavage reactions, supercoiled pUC19 plasmid DNA (form I, 40 μM) in Tris−HCl/NaCl (5:50 mM) buffer at pH 7.1 was treated with solutions of copper complexes. The samples were incubated for 4 h at 37 °C. A loading buffer containing 25% bromophenol blue, 0.25% xylene cyanol, and 30% glycerol (3 μL) was added, and electrophoresis was performed at 60 V for 5 h in Tris−acetate−EDTA (TAE) buffer (40 mM Tris-base, 20 mM acetic acid, 1 mM EDTA) using 1% agarose gel containing 1.0 μg/mL ethidium bromide. The gels were viewed in an Alpha Innotech Corporation Gel doc system and photographed using a CCD camera. Densitometric calculations were made using the AlphaEaseFC StandAlone software. The intensities of supercoiled DNA were corrected by a factor of 1.47 as a result of its lower staining capacity by ethidium bromide.[70] We measured the cleavage efficiency by determining the ability of the complex to convert the SC DNA to nicked NC form and LC form.

The decrease in intensity of form I (SC) or the increase in the intensity of form II (NC) was then plotted against catalyst concentrations, and these were fitted well with a single-exponential decay curve (pseudo-first-order kinetics) by the use of known equations.[80] For anaerobic experiments, deoxygenated water and anaerobic stock solutions were prepared. To identify the reactive oxygen species (ROS) involved in the cleavage reaction, we introduced the radical scavengers such as hydroxyl radical (DMSO, 10%), singlet oxygen (NaN_3, 100 μM), super oxide (SOD, 10 unit), and H_2O_2 (catalase, 0.1 unit). The reaction products were resolved on 1% agarose gel in TAE buffer. The ligation experiment involves incubating complex 4 with pUC19 DNA for 4 h and then aliquoting the cleaved fragments into two Eppendorfs. One of the aliquots was subjected to ligation using T4 DNA ligase at 16 °C for 24 h.

The DNA cleavage with added reductant was monitored, as in the case of the cleavage experiment without added reductant using agarose gel electrophoresis. Reactions using supercoiled pUC19 plasmid DNA (SC, 40 μM, in base pair) in Tris−HCl/NaCl (5:50 mM) buffer at pH 7.1 were treated with the metal complex (30 μM) and ascorbic acid (10 μM), followed by dilution with the Tris−HCl buffer to a total volume of 20 μL. The samples were incubated for 0.5 h at 37 °C, and gel electrophoresis was performed as described above.

For photocleavage studies, the reactions were carried out under illuminated conditions at 365 nm (12 W) monochromatic light source. In each experiment, the sample was incubated for 1 h at 37 °C and analyzed for the photocleaved products using gel electrophoresis, as discussed above. Reactions using supercoiled pUC19 plasmid DNA (SC, 40 μM, in base pair) in Tris−HCl/NaCl (5:50 mM) buffer at pH 7.1 were treated with the metal complex (25 μM), followed by dilution with the Tris−HCl buffer to a total volume of 20 μL. The inhibition reactions for the photonuclease studies were carried out at 365 nm using reagents (NaN_3, 100 μM; DMSO, 10%) prior to the addition of the complex. For the D_2O experiment, the same solvent was used for dilution to 18 μL.

Cell Viability Assay. The MTT assay was carried out as previously described.[81] Complexes **2**−**4**in the concentration range

(78) Sugimori, T.; Masuda, H.; Ohata, N.; Koiwai, K.; Odani, A.; Yamauchi, O. *Inorg. Chem.* **1997**, *36*, 576–583.

(79) (a) Sheldrick, G. M. *SHELXTL Reference Manual: Version 5.1*; Bruker AXS: Madison, WI, 1997. (b) Sheldrick, G. M. *SHELXS-97: Program for the Solution of Crystal Structure*; University of Göttingen: Göttingen, Germany, 1997. (c) Sheldrick, G. M. *SHELXS-97: Program for the Refinement of Crystal Structure*; University of Göttingen: Göttingen, Germany, 2007.

(80) Sreedhara, A.; Freed, J. D.; Cowan, J. A. *J. Am. Chem. Soc.* **2000**, *122*, 8814–8824.

of 0.05−50 μM dissolved in H_2O were added to the wells 24 h after seeding of 5×10^3 cells per well in 200 μL of fresh culture medium. After 24 and 48 h, 20 μL of MTT solution (5 mg/mL in phosphate-buffered saline (PBS)) was added to each well. The plates were wrapped with aluminum foil and incubated for 4 h at 37 °C. The purple formazan product was dissolved by the addition of 100 μL of DMSO to each well. The absorbance was monitored at 570 (measurement) and 630 nm (reference) using a 96-well plate reader (Bio-Rad, Hercules, CA). Data were collected for three replicates each and used to calculate the mean. The percentage inhibition was calculated, from this data, using the formula:

$$= \frac{\text{Mean OD of untreated cells(control)} - \text{Mean OD of treated cells}}{\text{Mean OD of untreated cells(control)}} \times 100$$

The IC values (40, 50, 60) were calculated using Table Curve 2D version 5.01.

Analysis of Cell Cycle Progression. Cells were seeded in a 25 cm^2 flask at a density of 1 3×10^6 cells/flask. After 24 h, complexes **3** and **4** at IC_{50} concentration were added to the respective flasks and incubated for 24 and 48 h. Cells were trypsinized, harvested, and fixed with 1 mL of cold 80% ethanol in test tubes and incubated at 4 °C overnight. After incubation, cells were centrifuged at 1500 rpm for 5 min, and the cell pellets were resuspended in 100 μL of propidium iodide (500 μg/mL) containing 100 μL of RNase A (10 mg/mL) (Sigma, MO). Then, the cells were incubated on ice for 30 min.[81] We analyzed cell cycle distribution by using FACScan (Becton-Dickinson, Sanjose, CA) with a 488 nm argon ion laser. The PI signals were collected using a 585/42 band-pass filter. The data were acquired and analyzed with Cell Quest software.

Hoechst 33258 Staining. We detected cell pathology by staining the nuclear chromatin of trypsinized cells (4.0×10^4/mL) with 1 μL of Hoechst 33258 (1 mg/mL, aqueous) for 10 min at 37 °C. Cells in suspension were stained with Hoechst 33258 to detect apoptosis.[82] A drop of cell suspension was placed on a glass slide, and a coverslip was laid over it to reduce light diffraction. At random, 300 cells were observed in a fluorescent microscope (Carl Zeiss, Jena, Germany) fitted with a 377−355 nm filter at 400× magnification, and the percentage of cells reflecting pathological changes was calculated. Data were collected for four replicates and were used to calculate the mean and the standard deviation.

Comet Assay. DNA damage was quantified adopting comet assay as previously described.[65,66] Assays were performed under red light at 4 °C. Cells used for the comet assay were sampled from a monolayer during the growth phase 24 h after seeding. Cells were treated with the copper(II) complexes at IC_{50} concentration, and cells were harvested by trypsinization process at 12 and 24 h. Normal agarose in PBS (200 μL of 1% solution) at 65 °C was dropped gently onto a fully frosted microslide, was covered immediately with a coverslip, and was placed over a frozen ice pack for ∼5 min. The coverslip was removed after the gel had set. The cell suspension from each cell fraction, in duplicate, was mixed with 1% low melting agarose at 37 °C in 1:3 ratio. This mixture (100 μL) was quickly applied on top of the gel, coated over the microslide, and allowed to set as before. A third coating of 100 μL 1% low melting agarose was given on the gel containing the cell suspension and allowed to set. After solidification of the agarose, the coverslips were removed, and the slides were immersed in ice-cold lysis solution (2.5 M NaCl, 100 mM Na_2EDTA, 10 mM Tris, NaOH: pH 10, 0.1% Triton X-100) and placed in a refrigerator at 4 °C for 16 h. All of the above operations were performed under low lighting conditions to avoid DNA damage due to light. The slides, after being removed from the lysis solution, were placed horizontally in an electrophoresis tank. The reservoirs were filled with electrophoresis buffer (300 mM NaOH, 1 mM Na_2EDTA, pH > 13) until the slides were just immersed in it. The slides were allowed to stand in the buffer for ∼20 min (to allow DNA unwinding), after which electrophoresis was carried out at 0.8 V/cm for 15 min. After electrophoresis, the slides were removed, washed thrice in neutralization buffer (0.4 M Tris, pH 7.5), and gently tapped to dry. Nuclear DNA was stained with 20 μL of ethidium bromide (50 μg/mL). Photographs were obtained using an epifluorescence microscope (Carl Zeiss). From each treatment, 200 cells were digitalized and analyzed with image analysis software (CASP software). The images were used to determine the DNA content of individual nuclei and to evaluate the degree of DNA damage representing the fraction of total DNA in the tail.

Analysis of DNA Fragmentation. The cells used for the DNA fragmentation analysis were sampled from a monolayer during the growing phase 24 h after seeding. The cells were treated with complexes **3** and **4** at IC_{50} concentration. After 12 and 24 h, approximately 5×10^5 cells were stirred with lysis buffer (20 mM EDTA, 100 mM Tris, pH 8.0, 0.8% [w/v] SDS). RNase (40 μg/mL) was added and incubated for 4 h at 37 °C. Subsequent incubation with proteinase K (50 μg/mL) was performed overnight at 50 °C. To the DNA samples was added 5 μL of 5× DNA loading buffer (30% glycerol, 0.25% bromophenol blue). The samples were loaded into dry wells of a 1.2% agarose gel in TBE containing 0.5 μg/mL ethidium bromide. The gel was ran at low voltage (35 V) until the loading dye had ran two-thirds of the way down the gel. The gel was finally visualized with a UV light and documented using Gel Doc system (Alpha innotech).

Acknowledgment. We thank the Department of Atomic Energy, Mumbai, India (grant no. 2003/37/25/BRNS) and the Council of Scientific and Industrial Research (01(2101)/07/EMR-II) for funding the research program. M.P. is a recipient of the Ramanna Fellowship of Department of Science and Technology, New Delhi. The EPR spectral facilities extended by Dr. P. Sambasiva Rao, Pondicherry University, Pondicherry, are gratefully acknowledged. The UV−vis and fluorescence spectral facilities in the department were created by funding from the Department of Science and Technology (DST-FIST), New Delhi, and the University Grants Commission (UGC-SAP), New Delhi.

Supporting Information Available: Crystallographic data, including Tables S1−S3 and Figures S1−S12 in CIF format. This material is available free of charge via the Internet at http://pubs.acs.org.

IC801144X

(81) Blagosklonny, M.; El-Diery, W. S. *Int. J. Cancer* **1996**, *67*, 386–392.
(82) Kasibhatla, G. P. A. H.; Finucane, D.; Brunner, T.; Wetzel, E. B.; Green, D. R. Protocol: Staining of Suspension Cells with Hoechst 33258 to Detect Apoptosis. In *Culture and Biochemical Analysis of Cells*; Spector, D. L., Goldman, R. D., Leinwand, L. A., Eds.; Cell: A Laboratory Manual, Vol. *1*; Cold Spring Harbor Laboratory Press: Cold Spring Harbor, NY, 2000.